UNIVERSITÀ
DEGLI STUDI
DI PADOVA

DIPARTIMENTO
DI INGEGNERIA
DELL'INFORMAZIONE

DIPARTIMENTO DI INGEGNERIA DELL'INFORMAZIONE

CORSO DI LAUREA IN INFORMATION ENGINEERING

Study of a communication and localization system based on visible light

Relatore:
Prof. Stefano Tomasin

Laureando:
Davide Dal Bo
2032509

ANNO ACCADEMICO: 2024/2025
Data di laurea: 19/11/2025

Alla mia famiglia

"La vita non è una corsa ma un tiro al bersaglio: non è il risparmio del tempo che conta, bensì la capacità di trovare un centro."

Susanna Tamaro

Contents

1 Introduction **1**
1.1 Indoor communication and localisation 1
1.2 VLCL system proposed 3

2 VLCL system model **5**
2.1 VLCL framework 5
2.1.1 Bandwidth and power control 7
2.2 Bias tee 8

3 VLC module **9**
3.1 Communication model 9
3.2 Complementary error function *erfc(x)* 11

4 VLL module **13**
4.1 A-DPDOA Localisation model 13
4.1.1 Differential phase-shift computation 15
4.1.2 I/Q components extraction 18
4.1.3 Distance computation 20
4.2 Hilbert transform 20

5 Adaptive transmission design **23**
5.1 Description of the transmission model 23
5.2 Joint optimisation algorithm 25
5.3 Water-filling method 27

6 System performance **29**

Conclusions **33**

Bibliography **36**

Abstract

Visible light communication (VLC) is an emerging technology capable of supporting a high transmission rate for indoor communications using existing lighting infrastructure. Paired with VLC, Visible light localisation (VLL) is used for high-accuracy indoor position estimation. One big problem of VLL is that it is very sensitive to random tilting of the receiver, which narrows the real-world applications. The paper "An Advanced Integrated Visible Light Communication and Localization System" has proposed a visible light-based communication and localisation (VLCL) system, which is robust against random tilting of the receiver and capable of adapting the transmission modulation and power allocation based on the localisation accuracy and communication requirements. This thesis aims to study and comprehend the VLCL system proposed in the paper and describe in more depth its functioning. The focus will be primarily on the advanced differential phase difference of arrival (A-DPDOA) localisation design and the adaptive transmission modulation.

Sommario

La comunicazione basata su luce visibile è una tecnologia emergente capace di supportare la trasmissione di dati ad alta velocità per comunicazioni in ambienti chiusi; il tutto utilizzando infrastrutture per l'illuminazione già presenti. Spesso annessa alla precedente, la localizzazione basata su luce visibile viene usata per stimare la posizione in ambienti chiusi. Un grosso problema della localizzazione basata su luce visibile è il fatto che è molto sensibile ad eventuali inclinazioni del ricevitore, il che ne riduce le possibili applicazioni. L'articolo "An Advanced Integrated Visible Light Communication and Localization System" ha proposto un sistema di comunicazione e localizzazione basato su luce visibile, il quale è resistente ad eventuali inclinazioni del ricevitore ed in grado di adattare la modulazione di trasmissione in base ai requisiti di comunicazione ed all'accuratezza nella localizzazione. Lo scopo di questa tesi è lo studio e la comprensione del sistema di comunicazione e localizzazione basato su luce visibile proposto nell'articolo, con una spiegazione a livello più approfondito del suo funzionamento. L'attenzione sarà rivolta principalmente al modello di localizzazione basato sulla differenza di fase all'arrivo differenziale avanzata e alla modulazione di trasmissione adattiva.

Chapter 1

Introduction

1.1 Indoor communication and localisation

Indoor communication and localisation systems are on the rise due to the increasing number of *Internet-of-Things (IoT)* devices in households, factories, hospitals, offices, and other indoor environments. In recent years, there have been many studies on *visible light communication (VLC)* and *visible light localisation (VLL)* systems as an alternative to *radio frequency (RF)* based systems.

VLC transmits data by modulating the intensity of light sources, such as light-emitting diodes (LEDs) and laser diodes (LDs). VLC merges lighting and data communications in applications such as indoor lighting, signboards, wireless local area networks, streetlights, vehicles, traffic signals, underwater signals, and so on.

The optical signal is then received by a photo-detector, which converts the light pulses back into electronic signals that can be decoded into data.

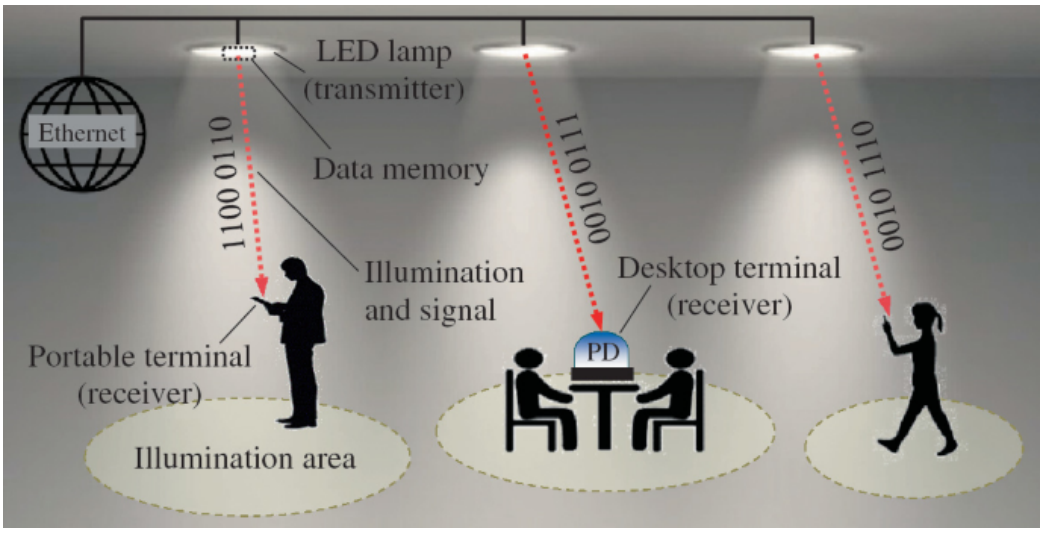

Figure 1.1: Example of a VLC system [1]

VLCL systems support the transmission of data at high speed, and the localisation protocol can be very helpful in environments where the devices need constant assistance in positioning, but there are some challenges to overcome:

1. Communication bands on the visible light spectrum leak interferences to adjacent bands, which reduces the communication performance and localisation accuracy.

2. When we have a limited amount of power, we have a tradeoff between VLC and VLL, and guaranteeing both the communication and localisation requirements becomes a challenge.

3. *Line-of-Sight (LoS)* blocking is an important issue in visible light systems, and designing a robust protocol to ensure data transmission and reception is also a challenge.

1.2 VLCL system proposed

The *Visible-Light Communication and Localisation (VLCL)* system proposed by [2] combines a *Orthogonal Frequency-Division Multiple Access (OFDMA)* modulation for the communication signal and an *Advanced Differential Phase Difference Of Arrival (A-DPDOA)* algorithm for the localisation. To control the localisation accuracy and fulfilment of *Quality-of-Service (QoS)* requirements, a joint adaptive modulation, subcarrier allocation and power allocation design is also proposed.

In this thesis, chapter 2 will describe the VLCL system model, while chapters 3 and 4 focus on the communication and localisation parts, respectively. In chapter 5, we will discuss the adaptive transmission design for the VLCL system. Chapter 6 reports the system performances and compares the accuracy of the localisation algorithm with respect to another model.

Chapter 2

VLCL system model

This chapter will describe the VLCL system proposed in [2] at a general level; it will also focus on some aspects that are not exclusive to the localisation or communication modules of the system.

2.1 VLCL framework

In figure 2.1(a), the physical implementation of the system is presented; the LED lamps transmit the data in addition to illumination, and the data is then received from the IoT device by a *Photo-Detector(PD)*, which transforms the visual light into a digital signal.

For the system diagram, we can refer to figure 2.1(b). On the transmission side, the communication signal, which is modulated following an OFDMA modulation, is summed to the localisation sine wave signals. Once these signals are generated for each LED lamp, they are then amplified and later combined with *direct current (DC)* voltage by bias-tees [2.2] to drive the

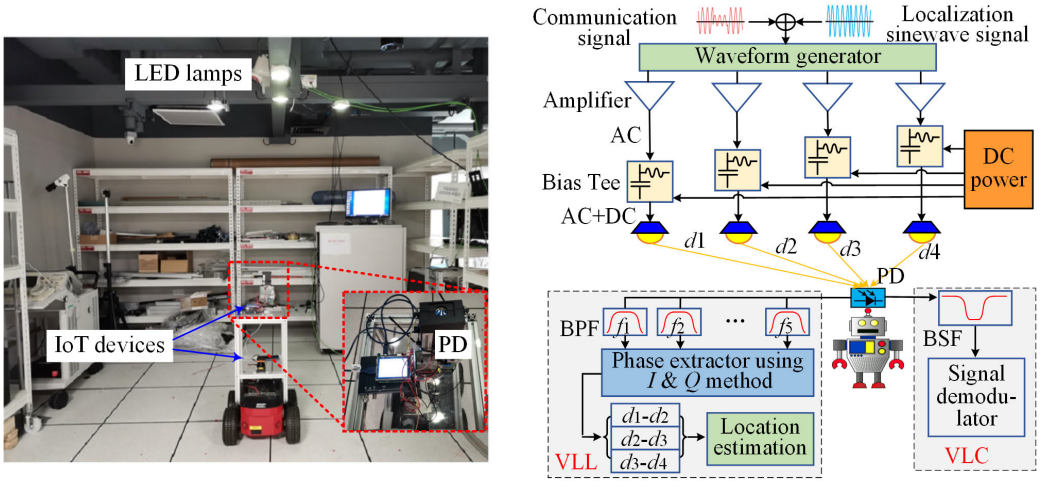

(a) Experiments conducted set up

(b) Block diagram of the integrated system.

Figure 2.1: System model of the integrated VLCL system [2]

corresponding LED lamps. The lamps transmit the data, which is received by the receiver by its PD; the optical signal is converted to digital, and then, through filtering, the communication signal is used by the VLC module and the localisation one by the VLL. The localisation signal is filtered using a series of *Band-Pass Filters (BPFs)*, one for each sine wave signal; the communication signal is extracted using a *Band-Stop Filter (BSF)*, which stops the frequency band where the localisation signal is present.

In figure 2.2, the electrical spectral density of the signal transmitted by each LED lamp is shown. In this case, we have 4 lamps and 5 different frequencies for the localisation signal, which are evenly distributed across the localisation frequency band; this is required for the A-DPDOA algorithm to work. The blue signal is the localisation one, while the red is the communication signal modulated by the OFDMA. From the image, we can see that there are five frequency holes in the communication signal spectrum; there we have

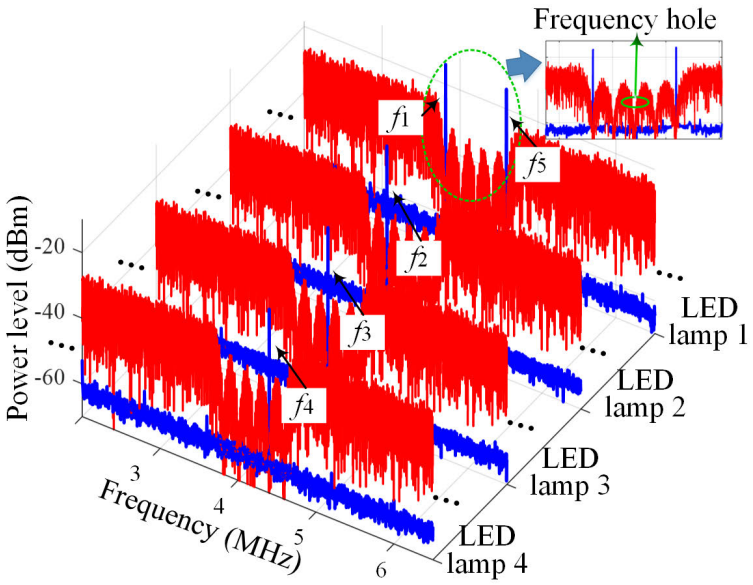

Figure 2.2: Electrical spectral density of the integrated signal [2]

negligible *Out-Of-Band Interference (OOBI)* from the adjacent communication subcarriers. We exploit this fact and place the localisation sinusoidal signals in these holes, avoiding interference that could lower the accuracy of the localisation.

2.1.1 Bandwidth and power control

Since the system is scalable, we can consider K general devices, all on the same floor. The total bandwidth is divided into N subcarriers; let F_L be the number of frequencies used for the localisation signals, the number of subcarriers applied to the communication is $N - F_L$. Since the system has K devices, and each device transmits data modulated by OFDMA, there is a need for K communication *Subcarrier Groups (SGs)*.

The power allocated to the communication and localisation subcarriers

must be balanced to respect the minimal positional accuracy and data rate. If we allocate more power to the VLC spectrum subcarriers, we can achieve a higher communication data rate, but we lose accuracy on the position; in contrast, if we allocate more power for the localisation, we get a lower data rate, since the received power signal is less. In order to achieve a trade-off, an adaptive transmission design is necessary.

2.2 Bias tee

A bias tee [3] is a three-port device used for setting a DC voltage bias of some electronic components without disturbing other components. The low-frequency port is used to insert the DC voltage components, while in the high-frequency port, the radio-frequency signal is passed. The combined port sees both the DC and RF signals. The bias tee gets its name from the design of the network, which is often arranged in a "T" shape.

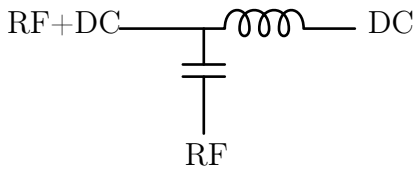

Figure 2.3: Equivalent circuit of a bias tee [4].

We can see it as an ideal capacitor that allows the DC component to pass and blocks the RF component, and an ideal inductor that does the opposite.

Chapter 3

VLC module

The communication model is based on the OFDMA modulation, which allows data to be transmitted at the same time, and with less frequency occupation, to multiple devices. Each device will have an amount of frequencies allocated exclusively to it, the number of frequencies and the power allocated to the device is selected by the adaptive transmission model.

3.1 Communication model

In a VLC system consisting of a LED lamp and a device connected to a PD, we can define the following variables:

- μ: the PD's resposivity
- $P_{n,i}$: the allocated electrical power on subcarrier n at LED i
- $H_{i,n,k}$: the *Line-of-Sight (LoS)* optical channel gain from LED i to device k on subcarrier n

- δ^2: the additive background noise power at the devices

With these we can define the received *Signal-to-Noise Ratio (SNR)* at device k on communication subcarrier n as

$$\gamma_{k,n}^{co} = \mu^2(\sum_{i=1}^{L} \sqrt{P_{n,i}} H_{i,n,k})^2/\delta^2. \tag{3.1}$$

For a device k assigned on the n-th subcarrier, the transmission signal can be modulated by a M_n-*Quadrature Amplitude Modulation (QAM)* with modulation order M_n. In this case the *Bit Error Rate (BER)* is defined as

$$BER_{k,n} = \frac{\sqrt{M_n} - 1}{\sqrt{M_n} log_2(\sqrt{M_n})} erfc(\sqrt{\frac{3\gamma_{k,n}^{co}}{2(M_n - 1)}}), \tag{3.2}$$

where the function $erfc(x)$ is the complementary error function, which is explained in the next section. The $BER_{k,n}$ is later needed to perform the power and subcarrier allocation algorithm.

Another requirement that we have to take into account is the data rate. To compute it, we need to know

- $\rho_{k,n}$: binary parameter, it shows us if the communication subcarrier n is allocated to device k, $\rho_{k,n} \in \{0, 1\}$, 1=allocated, 0=not allocated
- $B_{sub} = B/N$: subcarrier bandwidth, B denotes the communication transmission bandwidth

Once we know these values, we can compute the data rate of the k-th device R_k

$$R_k = B_{sub} \sum_{n=1}^{N/2-1} (\rho_{k,n} \log_2 M_n). \tag{3.3}$$

3.2 Complementary error function *erfc(x)*

To understand the complementary error function we have to know that $erfc(x)$ is defined as

$$erfc(x) = 1 - erf(x). \tag{3.4}$$

The error function, also called the Gauss error function, is defined as

$$erf(x) = \frac{2}{\sqrt{\pi}} \int_0^x e^{-t^2} dt = \frac{1}{\sqrt{\pi}} \int_{-x}^x e^{-t^2} dt \tag{3.5}$$

This means that $erf(x)$ gives the probability of a random variable, with normal distribution of mean 0 and variance $\frac{1}{2}$, to fall in the range $[-x, x]$. Then, $erfc(x)$ represents the probability of the same random variable to fall outside of the range $[-x, x]$.

Chapter 4

VLL module

The VLL module uses an advanced differential-phase difference of arrival as its localisation model. This approach is based on the *In-phase/Quadrature (I/Q)* demodulation of the received localisation signal to retrieve the phase shift of the localisation signals. The demodulation would usually require a *Local Oscillator (LO)* synchronised with the transmitted sinusoidal signal from each lamp, which would increase the complexity of the system and decrease its feasibility. The innovative aspect of this model is that it does not require a LO, since it uses the phase difference of arrival of the localisation signals by multiplying two different frequency signals.

4.1 A-DPDOA Localisation model

Set $d_{i,k}$ as the transmission distance between the i-th LED lamp and the k-th device, it can be written as $d_{i,k} = t_{i,k}c$, where c is the speed of light and $t_{i,k}$ is the propagation time.

The propagation time can be computed from the phase shift $\Delta\varphi_{i,k}$ of the signal and its frequency f_i as

$$t_{i,k} = \Delta\varphi_{i,k}/2\pi f_i. \tag{4.1}$$

Let $S_i^{Tx}(t)$ denote the input sinusoidal signal transmitted by lamp i, with φ_0 as the initial phase of the signal, $S_i^{Tx}(t)$ is expressed as

$$S_i^{Tx}(t) = \sqrt{P_i}\sin(2\pi f_i t + \varphi_0). \tag{4.2}$$

The signal is then propagated through an indoor optical wireless channel, received by the device and filtered through a BPF to isolate the localisation sinusoidal signal. In the transmission, the signal (4.2) is affected by $H_{i,k}$, the LoS optical wireless channel gain between device k and lamp i, and the background noise at device k, which is represented by $n_k(t)$. The received signal $S_i^{Rx}(t)$ at the k-th device is given by

$$S_{i,k}^{Rx}(t) = \sqrt{P_i}H_{i,k}\sin(2\pi f_i t + \Delta\varphi_{i,k} + \varphi_0) + n_k(t). \tag{4.3}$$

Using formula (4.1) and remembering $\omega = 2\pi f$, we can rewrite (4.3) as

$$S_{i,k}^{Rx}(t) = \sqrt{P_i}H_{i,k}\sin(\omega_i t + \omega_i t_{i,k} + \varphi_0) + n_k(t) \tag{4.4}$$

4.1.1 Differential phase-shift computation

At this point, instead of multiplying the received signal by the synchronised sinusoid that the LO would generate, we use the differential phase-shift approach.

Multiplying $S^{Rx}_{1,k}(t)$ by $S^{Rx}_{2,k}(t)$ and recalling that $\sin(a)\sin(b) = \frac{1}{2}[\cos(a-b) - \cos(a+b)]$, we get

$$\begin{aligned} S^{Rx}_{1,k}(t) \cdot S^{Rx}_{2,k}(t) &= [\sqrt{P_1}H_{1,k}\sin(\omega_1 t + \omega_1 t_{1,k} + \varphi_0) + n_k(t)]\cdot \\ &\qquad [\sqrt{P_2}H_{2,k}\sin(\omega_2 t + \omega_2 t_{2,k} + \varphi_0) + n_k(t)] \\ &= \frac{1}{2}\sqrt{P_1}\sqrt{P_2}H_{1,k}H_{2,k}[\cos(\omega_1 t + \omega_1 t_{1,k} + \varphi_0 - (\omega_2 t + \omega_2 t_{2,k} + \varphi_0)) - \\ &\qquad \cos(\omega_1 t + \omega_1 t_{1,k} + \varphi_0 + \omega_2 t + \omega_2 t_{2,k} + \varphi_0)] + n_{12,k}(t). \end{aligned}$$

where $n_{12,k}(t) = n_k^2(t) + n_k(t)[\sqrt{P_1}H_{1,k}\sin(\omega_1 t + \omega_1 t_{1,k} + \varphi_0) + \sqrt{P_2}H_{2,k}\sin(\omega_2 t + \omega_2 t_{2,k} + \varphi_0)]$ is the additive noise term from the two signals.

$$\begin{aligned} S^{Rx}_{1,k}(t) \cdot S^{Rx}_{2,k}(t) &= \frac{1}{2}\sqrt{P_1}\sqrt{P_2}H_{1,k}H_{2,k}[\cos((\omega_1 - \omega_2)t + \omega_1 t_{1,k} - \omega_2 t_{2,k}) - \\ &\qquad \cos((\omega_1 + \omega_2)t + \omega_1 t_{1,k} + \omega_2 t_{2,k} + 2\varphi_0)] + n_{12,k}(t) \\ &= \frac{1}{2}\sqrt{P_1}\sqrt{P_2}H_{1,k}H_{2,k}[\cos((\omega_2 - \omega_1)t - \omega_1 t_{1,k} + \omega_2 t_{2,k}) - \\ &\qquad \cos((\omega_1 + \omega_2)t + \omega_1 t_{1,k} + \omega_2 t_{2,k} + 2\varphi_0)] + n_{12,k}(t) \quad (4.5) \end{aligned}$$

From (4.5) we just need the phase-difference component, which is extracted by filtering the signal with a BPF with centre frequency of $(\omega_2 - \omega_1)$, as seen in figure 4.1.

After the signal is filtered and its noise ignored, supposing it is small

enough, the phase-difference term is represented as

$$D_{1,k}(t) = \frac{1}{2}\sqrt{P_1}\sqrt{P_2}H_{1,k}H_{2,k}\cos((\omega_2 - \omega_1)t - \omega_1 t_{1,k} + \omega_2 t_{2,k}), \qquad (4.6)$$

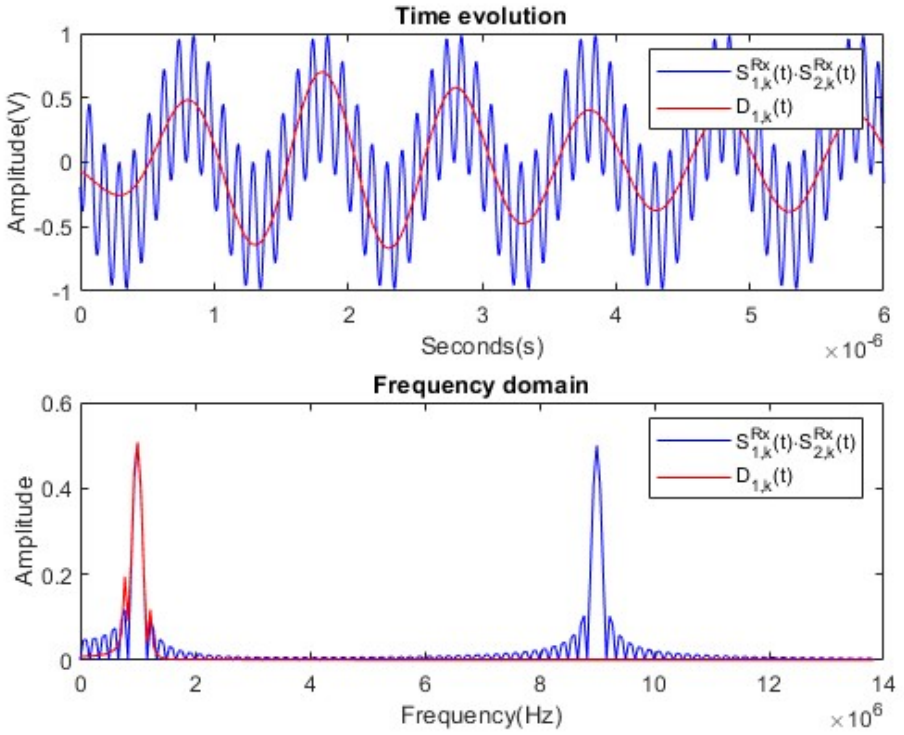

Figure 4.1: Example of signals ($f_1 = 4$ MHz and $f_2 = 5$ MHz)

The same equation, generalised, becomes

$$D_{i,k}(t) = \frac{1}{2}\sqrt{P_i}\sqrt{P_{i+1}}H_{i,k}H_{i+1,k}\cos((\omega_{i+1} - \omega_i)t - \omega_i t_{i,k} + \omega_{i+1} t_{i+1,k}). \quad (4.7)$$

To get the differential expression, we have to compute $D_{i,k}(t) \cdot D_{i+1,k}(t)$, taking as example $D_{1,k} \cdot D_{2,k}$ and recalling that $\cos(a)\cos(b) = \frac{1}{2}[\cos(a-b) + \cos(a+b)]$, we get

$$D_{1,k}(t)\cdot D_{2,k}(t) = \frac{1}{4}\sqrt{P_1}P_2\sqrt{P_3}H_{1,k}H_{2,k}^2H_{3,k}[\cos((\omega_2-\omega_1)t-\omega_1t_{1,k}+\omega_2t_{2,k})\cdot$$
$$\cos((\omega_3-\omega_2)t-\omega_2t_{2,k}+\omega_3t_{3,k})]$$
$$= \frac{1}{8}\sqrt{P_1}P_2\sqrt{P_3}H_{1,k}H_{2,k}^2H_{3,k}\cdot$$
$$[\cos((\omega_2-\omega_1)t-\omega_1t_{1,k}+\omega_2t_{2,k}-(\omega_3-\omega_2)t+\omega_2t_{2,k}-\omega_3t_{3,k})$$
$$+\cos((\omega_2-\omega_1)t-\omega_1t_{1,k}+\omega_2t_{2,k}+(\omega_3-\omega_2)t-\omega_2t_{2,k}+\omega_3t_{3,k})]$$
$$= \frac{1}{8}\sqrt{P_1}P_2\sqrt{P_3}H_{1,k}H_{2,k}^2H_{3,k}[\cos((2\omega_2-\omega_1-\omega_3)t-\omega_1t_{1,k}+2\omega_2t_{2,k}-\omega_3t_{3,k})+$$
$$\cos((\omega_3-\omega_1)t-\omega_1t_{1,k}+\omega_3t_{3,k})] \quad (4.8)$$

From (4.8), we can see that a combination of the pulsations plus some phase shift controls both the cosinusoidal components. To simplify the extraction of the I/Q components of the signals, [2] sets the pulsation of the first cosine to 0; this happens only if the localisation frequencies are separated by the same frequency-gap $\Delta f = \Delta\omega/2\pi$:

$$2\omega_2-\omega_1-\omega_3 = 0$$
$$2\omega_2 = \omega_1+\omega_3$$
$$2(\omega_1+\Delta\omega) = \omega_1+(\omega_1+2\Delta\omega)$$
$$2\omega_1+2\Delta\omega = 2\omega_1+2\Delta\omega \quad (4.9)$$

Imposing the frequencies to be equally divided, (4.8) becomes

$$D_{1,k}(t)\cdot D_{2,k}(t) = \frac{1}{8}\sqrt{P_1}P_2\sqrt{P_3}H_{1,k}H_{2,k}^2H_{3,k}[\cos(-\omega_1 t_{1,k}+2\omega_2 t_{2,k}-\omega_3 t_{3,k})+ \cos((\omega_3-\omega_1)t-\omega_1 t_{1,k}+\omega_3 t_{3,k})] \quad (4.10)$$

4.1.2 I/Q components extraction

To achieve the differential of phase differences, we have to extract the phase of (4.10). To get it, we extract the In-phase and Quadrature-phase components of the signal using a LPF and the Hilbert transform.

$$\begin{aligned} I_{1,k} &= LPF(D_{1,k}(t)\cdot D_{2,k}(t)) = \\ &LPF(\frac{1}{8}\sqrt{P_1}P_2\sqrt{P_3}H_{1,k}H_{2,k}^2H_{3,k}[\cos(-\omega_1 t_{1,k}+2\omega_2 t_{2,k}-\omega_3 t_{3,k})+ \\ &\qquad \cos((\omega_3-\omega_1)t-\omega_1 t_{1,k}+\omega_3 t_{3,k})]) \\ &= \frac{1}{8}\sqrt{P_1}P_2\sqrt{P_3}H_{1,k}H_{2,k}^2H_{3,k}\cos(\omega_1 t_{1,k}-2\omega_2 t_{2,k}+\omega_3 t_{3,k}) \quad (4.11) \end{aligned}$$

For the quadrature component, we use the Hilbert transform (in the equation we will use $Hilb(\cdot)$ instead of $H(\cdot)$ to not confuse it with the LoS optical channel gain $H_{i,k}$) to get the orthogonal signal of $D_{2,k}(t)$, which in this case changes the cosine to become a sine. Since $\cos(a)\sin(b) = \frac{1}{2}[\sin(a+b)+\sin(a-b)]$, the factors and arguments of $D_{2,k}(t)$ do not change, only the cosine is replaced by the sine.

$$
\begin{aligned}
Q_{1,k} &= LPF(D_{1,k}(t) \cdot Hilb(D_{2,k}(t))) = \\
&\quad LPF(\frac{1}{8}\sqrt{P_1}P_2\sqrt{P_3}H_{1,k}H_{2,k}^2H_{3,k}[\sin(-\omega_1 t_{1,k} + 2\omega_2 t_{2,k} - \omega_3 t_{3,k}) + \\
&\qquad\qquad \sin((\omega_3 - \omega_1)t - \omega_1 t_{1,k} + \omega_3 t_{3,k})]) \\
&\quad = \frac{1}{8}\sqrt{P_1}P_2\sqrt{P_3}H_{1,k}H_{2,k}^2H_{3,k}\sin(\omega_1 t_{1,k} - 2\omega_2 t_{2,k} + \omega_3 t_{3,k}) \quad (4.12)
\end{aligned}
$$

Taking the ratio $Q_{1,k}/I_{1,k}$, the amplitude terms are cancelled and we get a $\tan(\cdot)$ based phase term

$$
\begin{aligned}
Q_{1,k}/I_{1,k} &= \frac{\frac{1}{8}\sqrt{P_1}P_2\sqrt{P_3}H_{1,k}H_{2,k}^2H_{3,k}\sin(\omega_1 t_{1,k} - 2\omega_2 t_{2,k} + \omega_3 t_{3,k})}{\frac{1}{8}\sqrt{P_1}P_2\sqrt{P_3}H_{1,k}H_{2,k}^2H_{3,k}\cos(\omega_1 t_{1,k} - 2\omega_2 t_{2,k} + \omega_3 t_{3,k})} \\
&= \tan(\omega_1 t_{1,k} - 2\omega_2 t_{2,k} + \omega_3 t_{3,k}). \quad (4.13)
\end{aligned}
$$

From (4.13) we can extrapolate the phase as

$$
\omega_1 t_{1,k} - 2\omega_2 t_{2,k} + \omega_3 t_{3,k} = \tan^{-1}(Q_{1,k}/I_{1,k}). \quad (4.14)
$$

Similarly, we also get

$$
\omega_2 t_{2,k} - 2\omega_3 t_{3,k} + \omega_4 t_{4,k} = \tan^{-1}(Q_{2,k}/I_{2,k}), \quad (4.15)
$$

$$
\omega_3 t_{3,k} - 2\omega_4 t_{4,k} + \omega_5 t_{5,k} = \tan^{-1}(Q_{3,k}/I_{3,k}). \quad (4.16)
$$

4.1.3 Distance computation

To compute the distance between the lamps and the device, [2] uses a distance difference variable problem. Consider $d_{i,k} - d_{i+1,k}$ as a variable, where $d_{i,k} = t_{i,k}c$; rewriting from (4.14) to (4.16) into a matrix, we get

$$\begin{pmatrix} d_{1,k} - d_{2,k} \\ d_{2,k} - d_{3,k} \\ d_{3,k} - d_{4,k} \end{pmatrix} = c \begin{pmatrix} tan^{-1}(Q_{1,k}/I_{1,k}) \\ tan^{-1}(Q_{2,k}/I_{2,k}) \\ tan^{-1}(Q_{3,k}/I_{3,k}) \end{pmatrix} \begin{bmatrix} \omega_1 & -\omega_3 & 0 \\ 0 & \omega_2 & -\omega_4 \\ \omega_5 & \omega_5 & \omega_5 + \omega_3 \end{bmatrix}^{-1} . \quad (4.17)$$

Once the distance differences are computed, they are used to estimate the position of the device k with reference to the lamp i, with coordinate (x_i, y_i, z_i). From (4.11), (4.12) and (4.17) we observe that the distance difference variable $d_{i,k} - d_{i+1,k}$, depends by both the In-phase $I_{i,k}$ and Quadrature-phase $Q_{i,k}$ components, and they are related to the transmission power P_i. Thus, the variation of transmission power for the localisation signals can change the accuracy of the estimated position, affecting the localisation error.

4.2 Hilbert transform

The Hilbert transform is a mathematical operation that takes in input and gives as output a time-related function; it does not change the domain as a Fourier or Laplace transform. This transform induces a positive phase shift of $+90°$ for signals with negative frequencies, while if the signal has a positive frequency, the phase shift is of $-90°$.

To show its behaviour with frequency, we can use its relationship with the Fourier transform [5]. The Hilbert transform becomes a multiplier operator in the frequency domain, represented with $\sigma_H(\omega) = -i \cdot sgn(\omega)$, where $sgn(\cdot)$ is the signum function.

$$\mathcal{F}(H(u))(\omega) = -i \cdot sgn(\omega) \cdot \mathcal{F}(u)(\omega)$$

By Euler's formula, the phase-shift becomes a complex exponential, we then get that $\sigma_H(\omega)$ has the following values

$$\sigma_H(\omega) = \begin{cases} i = e^{+i\pi/2} & \text{if } \omega < 0 \\ 0 & \text{if } \omega = 0 \\ -i = e^{-i\pi/2} & \text{if } \omega > 0 \end{cases}$$

As said before, we can see that for negative frequency components of $u(t)$ the shift is of $\frac{\pi}{2}$ and for positive frequency it is $-\frac{\pi}{2}$. We note that if we apply the Hilbert transform twice, the components are shifted by $\pm 180°$, which results in a negation of the signal.

$$(\sigma_H(\omega))^2 = e^{\pm i\pi} = -1 \quad \text{for } \omega \neq 0.$$

Chapter 5

Adaptive transmission design

To fulfil data rate requirements and localisation accuracy, we have to control the power allocated for communication and localisation signals. To do so, [2] proposes a joint adaptive modulation, subcarrier allocation and power allocation.

5.1 Description of the transmission model

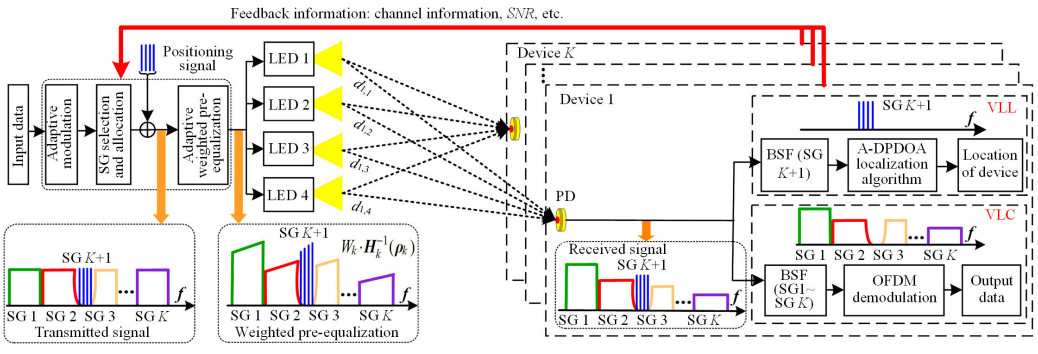

Figure 5.1: Block diagram of the proposed adaptive transmission for the integrated VLCL system. [2]

As we can see from figure 5.1, at the controller, the system allocates communication *Subcarrier Groups (SGs)* to the devices and then the localisation signals for VLL are integrated into the communication signal. The localisation frequencies are set in the $(K+1)$-th SG and all the communication signals are allocated on K SGs, one for each of the K devices. The controller receives the information about the channel state and quality and data rate requirements from each device, it then selects M-QAM mapping based on the minimum requirements and feedback information. To select the right modulation order M_n, the system bases its decision on the received SNR value $\gamma_{k,n}^{co}$ of device k. The selection process for M_n is

$$M_n = 2^j, \quad \gamma_j^{th} \leq \gamma_{k,n}^{co} \leq \gamma_{j+1}^{th}, \quad j = 1, ..., J-1, \tag{5.1}$$

where γ_j^{th} represents the SNR target value of the corresponding modulation level j. At the same time, the system checks that the current $BER_{k,n}$ is less than the maximum threshold BER_{max}.

From figure 5.1 we see that once the communication and localisation signals are integrated, they are amplified by an adaptive weighted pre-equalisation, to compensate for the frequency attenuation of LEDs in the high-frequency domain. This is done to receive at the devices a signal as close to the generated one as possible. To define the relation of the signal before and after pre-equalisation, we need to know:

- ρ_k: the continuous subcarrier allocation indicator

- M_k: denotes the modulation order of the k-th subcarrier group

- $S'_k(M_k, \rho_k)$: signal vector before pre-equalisation
- $S_k(M_k, \rho_k)$: signal vector after pre-equalisation
- P_k: the power allocation coefficient of the k-th subcarrier group
- H_k: transfer function matrix of SG k

With the values above, we can define the relation of the k-th SG signal in the frequency domain when considering the joint adaptive modulation, subcarrier allocation and power allocation as

$$S'_k(M_k, \rho_k) = \sqrt{P_k} \cdot H_k^{-1} \cdot S_k(M_k, \rho_k). \tag{5.2}$$

Once the signal is received by the device, it is separated in the localisation signal component using a BPF, and for the communication signal, a BSF is used, blocking the frequency band containing the localisation frequencies. Each device then demodulates its corresponding SG and retrieves the data that it needs.

After the data is received, the device sends back the feedback information about the channel state and its received SNR to the controller. Once the controller has the SNR value sent back, it can check if the QoS requirements are met. If they are not, we can use the water-filling method [5.3] to increase the power allocation value in the next iteration, increasing the data rate.

5.2 Joint optimisation algorithm

The joint optimisation algorithm can be described with the following steps:

- **Step 1:** Initialize the iteration $i = 0$, set the initial sum data rate $R_{sum}(0) = 0$, subcarrier allocation indicator $\rho_k(0)$, weighted pre-equalisation power coefficients $P_k(0)$ and modulation order $M_k(0)$ for each device. Set the maximum data rate tolerance $\varsigma \geq 0$

- **Step 2:** Each device k sends its detected channel information, localisation accuracy requirements and minimum data rate requirements R_k^{min} to the controller via WiFi or VLC uplink links.

- **Step 3:** The controller updates the weighted pre-equalisation coefficients $P_{k+1}(0)$ on localisation SG to guarantee localisation accuracy first.

- **Step 4:** Following the data rate minimum requirements, the controller iteratively computes the subcarrier allocation indicator $\rho_k(0)$, weighted pre-equalisation power coefficients $P_k(i+1)$ and modulation order $M_k(i+1)$ for each device, allocating enough communication resource to satisfy $R_k(i) \geq R_k^{min}$.

- **Step 5:** After the minimum data rates are ensured, the extra power is allocated to the devices with the best channel quality to maximise the sum data rate $R_{sum}(i+1)$ by updating $\rho_k(i+1)$, $P_k(i+1)$ and $M_k(i+1)$.

- **Step 6:** Set $i = i + 1$ and update the sum data rate $R_{sum}(i)$.

- **Step 7:** Repeat from Step 2 to Step 6 until the difference of the summed data rate between each interaction is less than the maximum data rate tolerance $|R_{sum}(i) - R_{sum}(i-1)| \leq \varsigma$.

- **Step 8:** The controller outputs the parameters $\rho_k(i)$, $P_k(i)$ and $M_k(i)$ to check their values.

5.3 Water-filling method

The water-filling algorithm [6] is a technique used for allocating optimal power among different channels in multicarrier schemes. It is known as water-filling as its process resembles how the water fills a container with an uneven bottom. We can think of the communication medium as if it were a water container with an irregular and asymmetrical bottom. Each channel is a portion of the container, having its own depth. To allocate power, we imagine pouring water into the container. The amount of water depends on the available power to allocate. Each section will contain a quantity of water based on the depth of its bottom; most of the water will be in the sections with a lower bottom, as we can see in figure 5.2. This translates to a higher allocation of power in the channels with lower interference, resulting in a higher SNR.

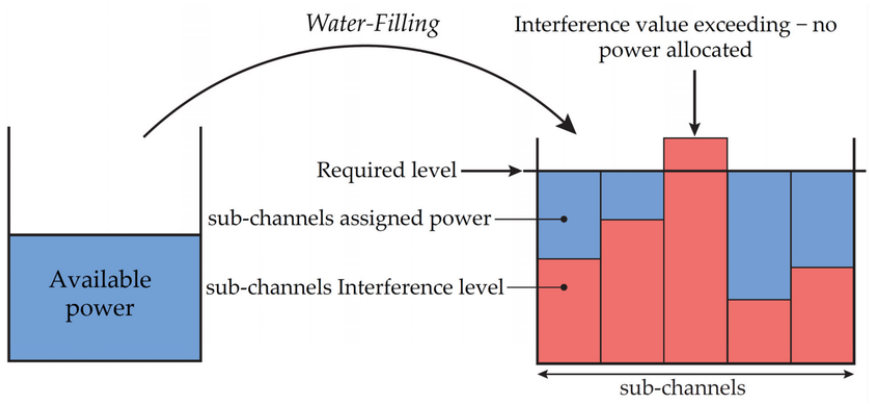

Figure 5.2: Principle of the water-filling algorithm [7]

Chapter 6

System performance

The following performances were achieved with:

- Coverage area of 222.5 m^3
- Inverse Fast Fourier Transform size $N = 256$
- Modulation bandwidth of 20 MHz
- Modulation order $M = \{2, 4, 8, 16, 32, 64\}$
- $BER_{max} = 3.8 \cdot 10^{-3}$
- Frequencies of the five sinusoidal signals for localisation range from 4.0 to 4.8 MHz, with each frequency gap being 0.2 MHz

The localisation algorithm has been tested in 2D and 3D location estimation at heights of 1.2 m, 1.5 m and 1.8 m; their mean estimation errors are 4.8 cm, 5.9 cm and 6.7 cm, respectively, for the 2D estimation. For the 3D estimation, the mean estimation error at the heights of 1.2 m, 1.5 m and 1.8 m are 10.8 cm, 9.5 cm and 8.0 cm, respectively.

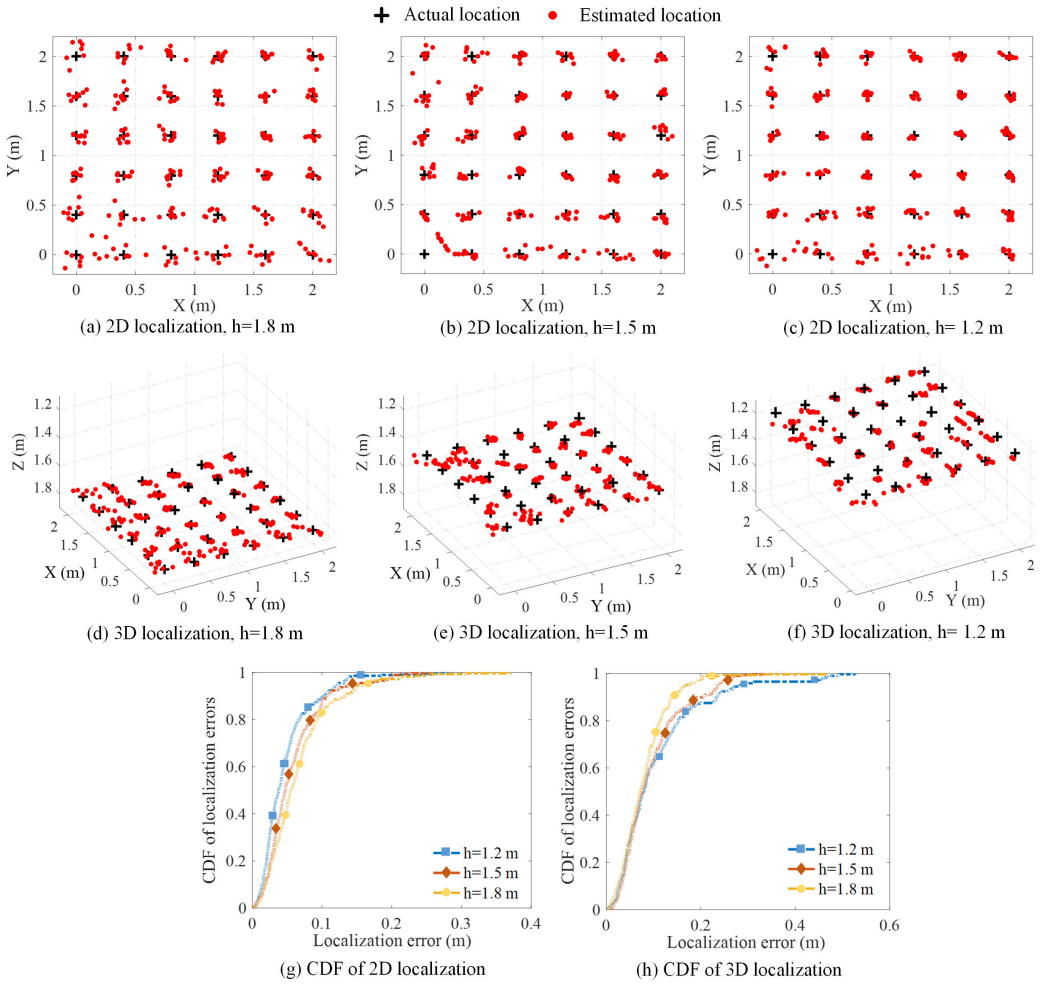

Figure 6.1: Comparisons of localisation results and localisation errors' *Cumulative Distribution Function (CDF)* [2]

As we can see from the *Cumulative Distribution Function (CDF)* at figure 6.1(g), at height 1.5 m, the location errors are less than 10 cm in 90% of the estimation; at the same height, for the 3D localisation, the localisation errors are less than 20 cm in 90% of the cases. This verifies the accuracy of the localisation algorithm.

Concerning the robustness of the algorithm under PD random tilting, the localisation estimations have been compared with a *Received Signal Strength*

(RSS) model; the results are shown in figure 6.2.

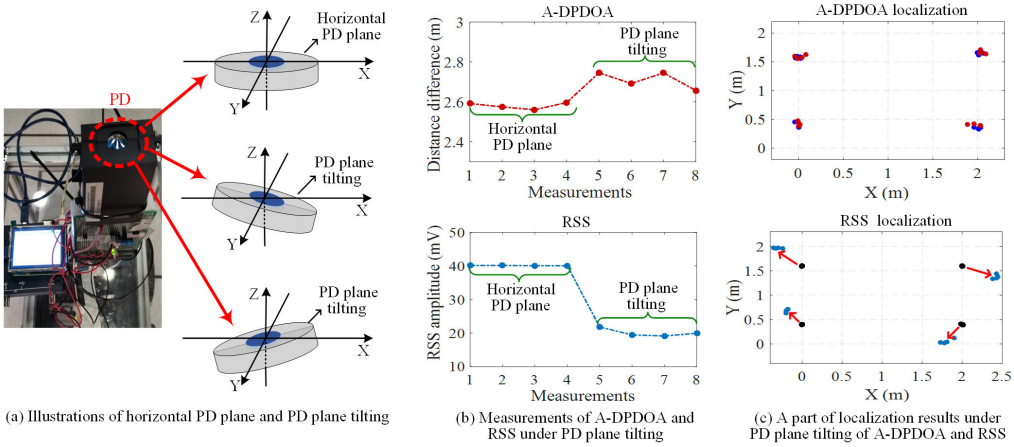

(a) Illustrations of horizontal PD plane and PD plane tilting

(b) Measurements of A-DPDOA and RSS under PD plane tilting

(c) A part of localization results under PD plane tilting of A-DPDOA and RSS

Figure 6.2: Measurements under random tilting of PD plane [2]

In the figure above, we can see that the RSS method is much more susceptible to the PD plane tilting, which is easily noticeable in figure 6.2(c); the estimated locations of A-DPDAO(red dots) are very close to the actual locations in presence of PD plane tilting, while the estimated locations of the RSS(blue dots), deviate from the actual locations.

The higher accuracy of the A-DPDOA can also be seen in figure 6.3, where, while moving the device around the uneven floor, the PD is affected by some tilting, which causes the location estimation to have a high error.

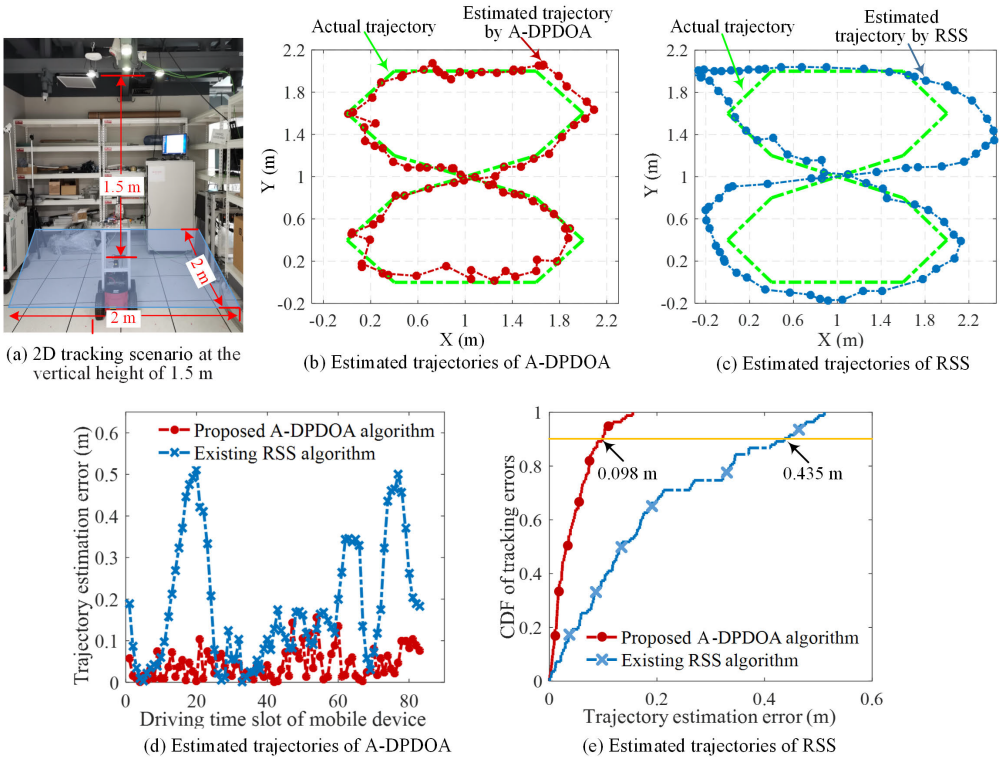

Figure 6.3: 2D tracking measurements under random tilting of PD plane [2]

Conclusions

In this thesis, we analysed a VLCL system, dividing it into its principal components. We saw the framework, how the signal is transmitted by the LED lamps and the separation of the signals for the communication and localisation modules.

We listed the characteristics of the communication module, which are used to control the modulation order and the power and frequency allocation by the adaptive transmission algorithm. We explained how the localisation signal is processed and the advantages of the proposed model, the principal being that, with its A-DPDOA model, it does not require a LO inside the receivers, keeping the system complexity to a minimum and ensuring localisation accuracy. The transmission is controlled by an algorithm, which takes into account the state of the wireless optical channel and the QoS requirements. The algorithm adjusts the power and frequency allocation, as well as the modulation order, of the signals to meet those requirements. It also modulates the amplitude of the signals transmitted to balance the frequency attenuation of the LEDs. Finally, we saw how the system performs and the comparison of its localisation model with one used in other systems, highlighting how the A-DPDOA model is much more robust and reliable.

Bibliography

[1] X. Lin, *VLC Current Applications*, pp. 109–124. Cham: Springer Nature Switzerland, 2025.

[2] H. Yang, S. Zhang, A. Alphones, C. Chen, K.-Y. Lam, Z. Xiong, L. Xiao, and Y. Zhang, "An advanced integrated visible light communication and localization system," *IEEE Transactions on Communications*, vol. 71, no. 12, pp. 7149–7162, 2023.

[3] Wikipedia contributors, "Bias tee — Wikipedia, the free encyclopedia." `https://en.wikipedia.org/w/index.php?title=Bias_tee&oldid=1320223217`, 2025. [Online; accessed 5-November-2025].

[4] Vgrimaldi94, "Equivalent circuit of a bias tee," 2007. License: CC BY-SA 4.0.

[5] Wikipedia contributors, "Hilbert transform — Wikipedia, the free encyclopedia." `https://en.wikipedia.org/w/index.php?title=Hilbert_transform&oldid=1312222309`, 2025. [Online; accessed 5-November-2025].

[6] H. Kour, R. K. Jha, and S. Jain, "A comprehensive survey on spectrum sharing: Architecture, energy efficiency and security issues," *Journal of Network and Computer Applications*, vol. 103, pp. 29–57, 2018.

[7] Wikipedia contributors, "Broadband power line communication for integration of energy sensors within a smart city ecosystem - scientific figure on researchgate.." https://www.researchgate.net/figure/Principle-of-Water-Filling-algorithm-76$_fig2_351585798$. [$Online; accessed 6 Nov 2025$].

Ringraziamenti

Vorrei ringraziare il mio relatore, il professor Stefano Tomasin, per il supporto e la pazienza avuta nei miei confronti. Un grazie ai compagni di corso, per aver fatto gruppo ed esserci aiutati a vicenda in questi anni ed aver reso la vita universitaria più leggera. Un grazie d'obbligo va alla mia famiglia, ai miei genitori che non mi hanno fatto pesare gli esami che non andavano bene e mi hanno sempre spinto ad andare avanti; a mio fratello, che con la sua costanza e determinazione nel seguire l'Università mi ha molte volte ispirato fiducia nel poter superare gli esami più ostici. Infine un grazie ai miei amici, per i bei momenti passati insieme pieni di risate ed il supporto incondizionato.